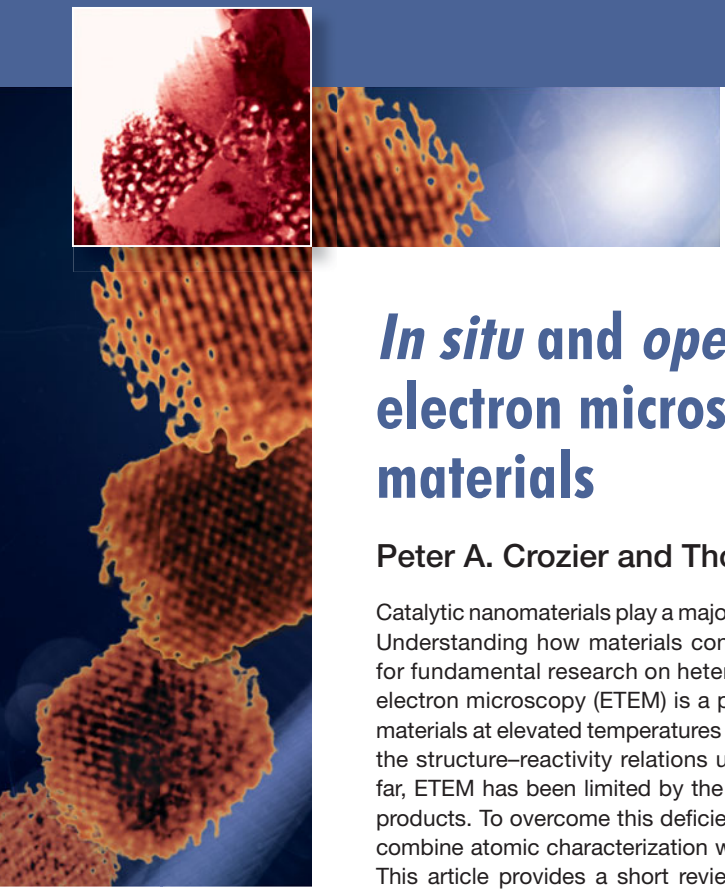


In situ and *operando* transmission electron microscopy of catalytic materials

Peter A. Crozier and Thomas W. Hansen

Catalytic nanomaterials play a major role in chemical conversions and energy transformations. Understanding how materials control and regulate surface reactions is a major objective for fundamental research on heterogeneous catalysts. *In situ* environmental transmission electron microscopy (ETEM) is a powerful technique for revealing the atomic structures of materials at elevated temperatures in the presence of reactive gases. This approach can allow the structure–reactivity relations underlying catalyst functionality to be investigated. Thus far, ETEM has been limited by the absence of *in situ* measurements of gas-phase catalytic products. To overcome this deficiency, *operando* TEM techniques are being developed that combine atomic characterization with the simultaneous measurement of catalytic products. This article provides a short review of the current status and major developments in the application of ETEM to gas-phase catalysis over the past 10 years.

Introduction

Heterogeneous catalysis is a key process for converting reactants into products, and it plays a critical role in chemical and energy transformations.[1,2] An industrial heterogeneous catalyst typically consists of nanostructured particles of variable shape and composition. The surfaces of catalytic particles interact with gas- or liquid-phase reactants and promote product generation. Reactions typically take place at temperatures up to 1000°C. As the catalytic materials convert gas- or liquid-phase reactants into products, the ambient gas or liquid environment also changes the surface and even the bulk form of the nanoparticles. During catalysis, the structure of the catalyst can vary in complex ways with changes in the pressures of the reactants and products as well as in the temperature. To build a structure–reactivity–performance correlation and achieve a fundamental understanding of catalytic mechanisms, the electronic and geometric structure of the catalyst must be determined at the atomic level. Environmental transmission electron microscopy (ETEM) is the only high-spatial-resolution technique available to perform *in situ* characterization of high-surface-area catalysts. In this approach, reactants are allowed to flow over the TEM sample (often during *in situ* heating), and the changes in the nanocatalyst particles are recorded using TEM imaging, diffraction, or spectroscopy techniques.

Catalysts are dynamic entities that change not only during each reaction cycle, but also on a longer time scale through phase transformations, surface restructuring, and particle growth. An example of this is illustrated in **Figure 1**, which shows a supported Ru catalyst for ammonia synthesis. In a vacuum, each Ru particle is encapsulated in a shell of BN, but under a reactive environment, this shell is no longer present.[3]

To build a direct correlation between catalyst structure and catalytic performance, structural information at the atomic or nanoscale level obtained under reaction conditions is critical. The value of the ETEM approach for characterizing high-surface-area materials was recognized by early workers in the field. Baker and co-workers were the first to extensively apply the technique to heterogeneous catalysts in a series of early works, elucidating the nanoscale mechanisms for carbon formation and catalyst sintering.[4,5] In the current article, we limit ourselves to select examples drawn mostly from the past 10 years focusing on gas-phase reactions/products. For reviews of earlier work, see References 6–9.

Atomic-resolution environmental *in situ* microscopy

A critical technical requirement for all gas systems compatible with TEM is that they maintain both a high gas pressure around a sample and a high vacuum throughout most of the

Peter A. Crozier, School of Engineering of Matter, Transport and Energy, Arizona State University, USA; crozier@asu.edu
Thomas W. Hansen, Center for Electron Nanoscopy, Technical University of Denmark, Denmark; twh@cen.dtu.dk
DOI: 10.1557/mrs.2014.304

© 2015 Materials Research Society
https://doi.org/10.1557/mrs.2014.304 Published online by Cambridge University Press

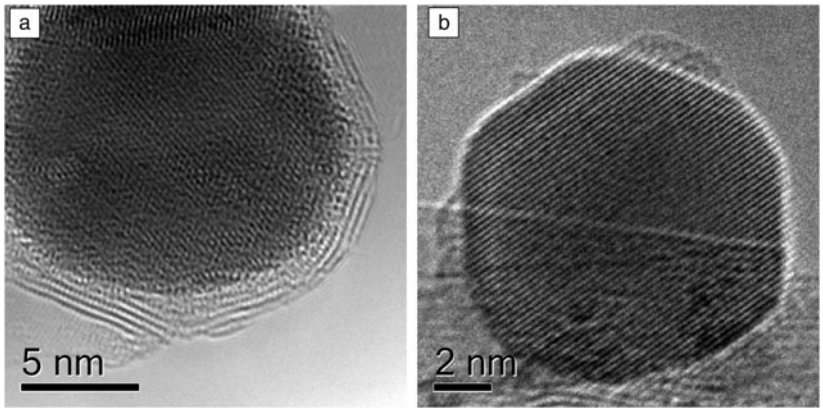


Figure 1. Boron nitride (BN) supported ruthenium particles.[3] (a) In a vacuum, the BN support creates shells encapsulating the metal particles. (b) When exposed to a reactive environment of N_2 and H_2 at 552°C, the shells are removed. Reproduced with permission from Reference 3. © 2001 American Association for the Advancement of Science.

column and the electron source. Two common approaches are currently employed to satisfy this requirement: the window method and differential pumping.

In the window method, thin electron-transparent membranes (e.g., Si_3N_4 or graphene films) are employed to separate the high-pressure atmosphere around the sample from the high vacuum in the rest of the microscope. This is usually accomplished by means of a sample holder that incorporates windows along with a gas inlet and outlet system. Atomic resolution has been demonstrated with such a system.[10,11] Recent application of microelectromechanical systems (MEMS) technology has resulted in the development of structures in which the area of the thin window is rather small, typically ~50 μm across, permitting higher pressure to be maintained (**Figure 2**a). A group at the Technical University of Delft first demonstrated an atomic resolution of 0.18 nm at pressures above 1 atm (~10^5 Pa ~1 Bar) and temperatures up to 500°C.[12] Prior to the development of MEMS windows, differentially pumped systems typically reached only between 10 and 20 mbar. Recent results showed that controlled-atmosphere experiments with windowed cells can be performed at pressures up to 4 atm (~4 bar) and elevated temperatures.[13,14] The issue of temperature measurement when a gas of variable pressure and composition is introduced is an ongoing challenge in MEMS-based windowed cells. Approaches are being developed that exploit changes in membrane conductivity and changes in the gas density to address this issue.[15]

The second approach to creating a reactive gas atmosphere is to employ a differentially pumped system; historical reviews of this approach can be found elsewhere.[9,16] Modern differential pumping systems are designed following the basic principles outlined by Swann and Tighe.[17] In this type of cell, the large pressure difference between the sample area and the microscope column is maintained by inserting a series of differential pumping apertures and adding additional pumping capacity. Atomic resolution was first achieved by a group at the University of Oxford on a modified JEOL 4000 instrument,[18] and the approach was continuously developed throughout the 1990s, often by means of substantial modification of the objective-lens pole pieces, as pioneered by Boyes and Gai.[19–21] Differential pumping systems compatible with field-emission electron sources were demonstrated,[22] and modern systems with aberration correction are currently available.[16,23]

A schematic diagram of a differentially pumped system is shown in Figure 2b. The microscope column (FEI Titan) has been modified to add three sets of differential pumping apertures for three pumping stages between the gun valve and viewing chamber. The first two sets of apertures are placed within the upper and lower objective-lens pole pieces, and most of the gas leaking through this first set of apertures is pumped out using a turbomolecular pump. The second stage is

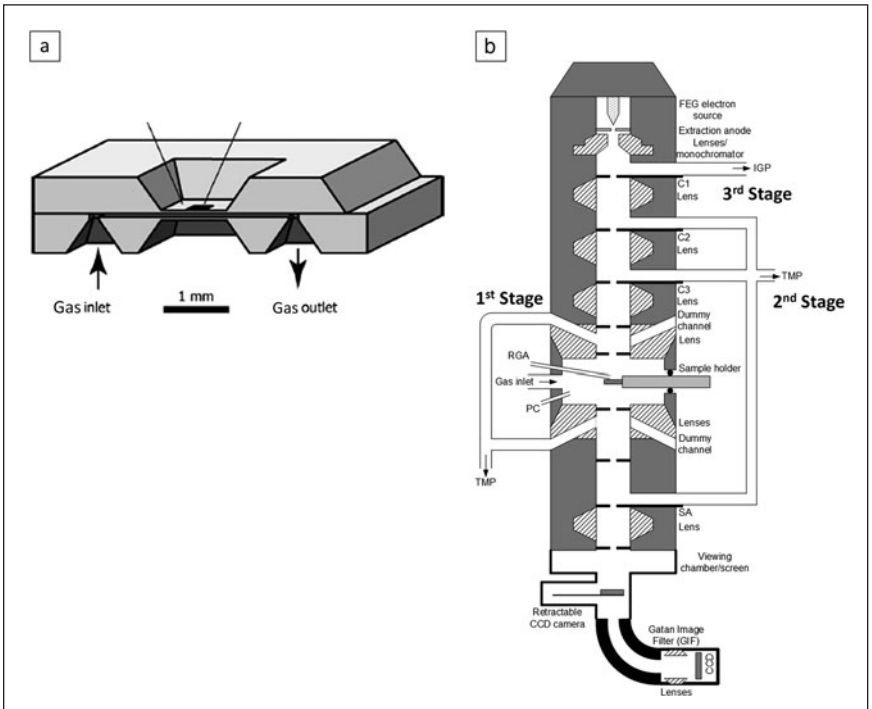


Figure 2. (a) Schematic diagram of a microelectromechanical systems-based windowed cell reactor.[12] (b) Schematic diagram of a differentially pumped environmental transmission electron microscopy apparatus.[16] Note: CCD, charge-coupled device; FEG, field-emission gun; IGP, ion getter pump; PC, plasma cleaner; RGA, residual gas analyzer; SA, selected-area aperture; TMP, turbomolecular pump.

https://doi.org/10.1557/mrs.2014.304 Published online by Cambridge University Press

between the condenser aperture and selected-area aperture and is pumped using a second turbomolecular pump. An additional ion pump is employed for the last stage before the gun valve.

Atomic-scale structural changes during gas exposure

Catalyst preparation

Catalyst preparation often involves oxidation and reduction treatments of metal precursors to generate dispersions of metallic nanoparticles on high-surface-area supports such as Al_2O_3, SiO_2, and TiO_2. ETEM has also been employed to follow the evolution of metal-supported catalysts during calcination and reduction. One advantage of the ETEM approach is that it allows the spatial distributions of the metal precursor, intermediate oxide, and final metal to be correlated from the same region of the catalytic material. Li et al. followed the evolution of a variety of metallic systems (Ni, NiCu, Co, and CoRu) prepared using impregnation techniques and high-surface-area supports.[24] The ability to perform *in situ* high-spatial-resolution electron energy-loss spectroscopy (EELS) in STEM mode is very beneficial in the study of bimetallic systems, where compositional heterogeneity might not be apparent from the TEM or STEM images.

For example, compositionally distinct domains in a 5-nm NiCu particle were observed in H_2 at 300°C, demonstrating the promotional effect of Cu in reducing NiO to Ni metal in bimetallic particles.[24] Banerjee and Crozier also undertook an investigation of the preparation of model Ni catalysts supported on SiO_2 spheres during both the calcination and reduction steps.[25] The simple geometry of this support made it easier to see metal diffusion during reduction and demonstrated that, for this system, finer metal dispersions were obtained by eliminating the calcination step and performing a direct reduction in H_2.

Dehghan et al. investigated the reducibility of cobalt oxide on 12 wt% Co/α-Al_2O_3 with and without a 0.5 wt% Re promoter.[26] Using imaging and EELS, they were able to show that, in 3 mbar of H_2, the initial Co_3O_4 started to transform to CoO at 180°C, and Co metal started to appear at 260°C, with complete reduction at 360°C. A similar result was also found for a CoO_x/SiO_2 composite system, which also exhibited nucleation and growth of metal particles during reduction.[27]

Catalyst activation can be thought of as a process taking place inside a reactor that leads to the formation of catalytically active species with the desired activity and selectivity. For example, the as-prepared anode on a solid-oxide fuel cell is often composed of a composite consisting of NiO and yttria-stabilized zirconia (YSZ). The fuel cell anode must be activated by reducing the NiO to Ni metal, which then acts as both a current collector and a catalyst. ETEM has been employed to follow the evolution of the anode under both reducing and oxidizing conditions.[28] **Figure 3** shows the evolution of the anode during a reduction and oxidation cycle. The initially dense NiO grains convert to a porous Ni metal structure during reduction (due to the volume shrinkage associated with the oxide-to-metal phase transformation). Interestingly, during reoxidation, NiO forms void-like structures, leading to an overall expansion in the NiO phase compared to the original NiO, which results in strain in the adjacent YSZ grains, as seen in Figure 3, and eventually leads to anode failure.

Structural evolution under reaction conditions

This broad category focuses on performing *in situ* imaging, spectroscopy, and diffraction on metal and oxide catalysts under near-reaction conditions. Some of the examples discussed next illustrate how the catalytic structure can change upon exposure to reactive gases and how structure can be correlated with reactivity.

Gold for CO oxidation

Au nanoparticles have received considerable attention because of their high activity for CO oxidation.[29] Giorgio and co-workers conducted several studies on the shape of Au nanoparticles on MgO, TiO_2, and carbon supports in 1 mbar of O_2, H_2, and CO + O_2 at room temperature.[10,30] Exposure to H_2 resulted in the particles assuming truncated octahedral shapes bounded by (111) and (100) facets, whereas exposure to O_2 resulted in the particles assuming a more rounded shape. This behavior was interpreted to indicate that O_2 chemisorbs at edges and defect sites. They repeated these experiments for CO oxidation and found that the Au particles were also predominantly round when CO_2 was produced.

Takeda's group has investigated the structure of Au particles on CeO_2 at room temperature in the presence of CO and O_2.[31] They also found that truncated octahedra formed when CO was present, and more rounded shapes formed in the presence of only oxygen (or air). Interestingly, even very low concentrations of CO mixed with oxygen stabilized the (111)

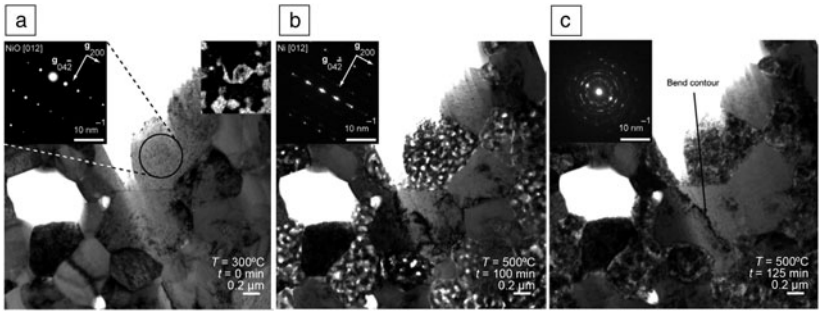


Figure 3. *In situ* reduction and reoxidation of a Ni/yttria-stabilized zirconia (YSZ) fuel-cell anode:[28] (a) initial structure composed of NiO/YSZ, (b) fully reduced anode showing porous Ni metal regions, and (c) reoxidized anode showing formation of porous NiO regions and a bend contour in YSZ, indicative of strain. Insets are electron diffraction patterns and an Ni elemental map. Reproduced with permission from Reference 28. © 2010 Elsevier Limited.

https://doi.org/10.1557/mrs.2014.304 Published online by Cambridge University Press

and (100) facets on Au, presumably because of the much larger chemisorption energy of CO compared to O_2. Under CO oxidation conditions, predominantly faceted particles with slightly rounded corners were observed. The same group recently repeated some of this work using aberration-corrected ETEM in 1 vol% CO in air (0.5 mbar) at room temperature.[32] They observed an outward relaxation of about 0.5 Å of the top (100) layer in the presence of CO (see **Figure 4**). When ETEM was performed at 80 kV, the sensitivity to light atoms was increased. Contrast on the surface of the Au nanoparticles was observed that appeared to be consistent with direct imaging of CO adsorbates. This might open up the exciting possibility of directly imaging gas adsorbates on the surfaces of nanoparticles.

Structure–reactivity relations from ETEM

Phase changes in Ni catalysts have also been correlated directly with catalytic activity for hydrocarbon reforming. Chenna and co-workers[33,34] used ETEM to determine the phase changes taking place on Ni/SiO_2 catalysts during temperature ramping and correlated these structural changes with changes in activity and selectivity determined by *ex situ* reactor studies. During ramping in 1.5 mbar of $2CH_4 + O_2$, at 400°C, the initial metallic Ni particles convert to NiO particles showing Kirkendall voids (see **Figure 5**). The NiO catalyzes complete oxidation of CH_4, resulting in the production of CO_2 and H_2O. As the temperature continues to rise, all of the oxygen in the reactor is converted, and the atmosphere becomes reducing, such that the NiO is reduced back to Ni metal at about 700°C. At this point, reforming begins, and the products change from CO_2 and H_2O to CO and H_2. The major changes in catalyst selectivity that appear at 400°C and 700°C correlate precisely with structural transformations determined by ETEM. The structure–reactivity relation derived from ETEM is shown schematically in the inset of Figure 5b.

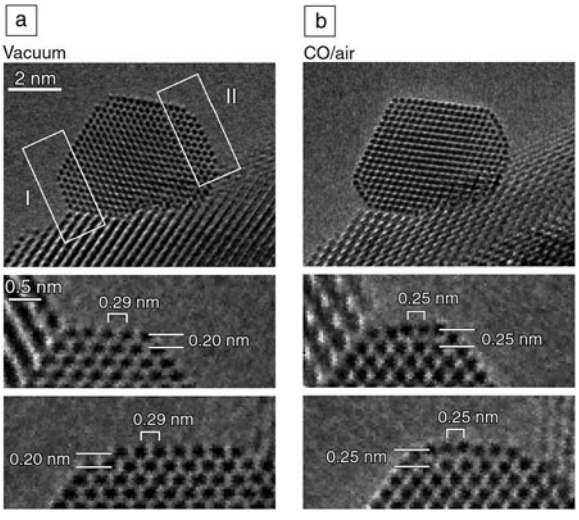


Figure 4. Gold nanoparticles supported on cerium oxide in (a) a vacuum and (b) a mixture of CO and air.[32] The middle and bottom rows show magnified images of the facets labeled I and II, respectively. When exposed to the CO gas mixture, the top-most Au layer on the {100} facets (indicated by white rectangles, top row) expands by 0.05 nm (middle and bottom rows). Reproduced with permission from Reference 32. © 2012 American Association for the Advancement of Science.

Oxides

Reducible oxides undergo changes in reactive atmospheres, often associated with Mars–van Krevelen-type mechanisms, in which oxygen for a reaction with an adsorbate comes directly from the oxide lattice. Consequently, there has been interest in exploring the changes that take place in oxides under

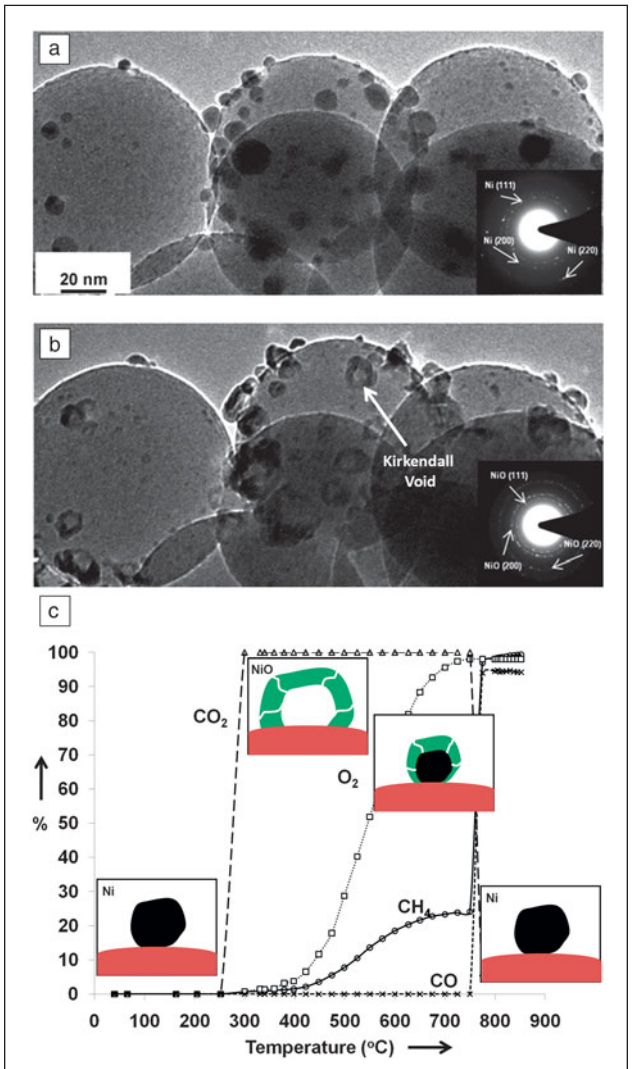


Figure 5. *In situ* environmental transmission electron microscope images and electron diffraction patterns of Ni/SiO_2: (a) in the presence of 1.5 mbar of H_2 at 400°C and (b) from the same region in the presence of 1.5 mbar of a mixture of CH_4 and O_2 in a 2:1 ratio at 400°C. (c) Structure–reactivity relations showing schematic diagrams of catalyst structure superimposed on catalytic data. The catalytic data show O_2 and CH_4 conversion along with selectivities for CO and CO_2.[33] Reproduced with permission from Reference 33. © 2011 Wiley-VCH Verlag GmbH&Co, KGaA, Weinheim.

https://doi.org/10.1557/mrs.2014.304 Published online by Cambridge University Press

redox conditions. Whereas catalysis takes place on the surface, the introduction or elimination of oxygen vacancies on the surface can be influenced by processes taking place in the bulk. Ceria is an interesting oxide in which Ce can exist in the 3+ or 4+ oxidation state. In a reducing atmosphere, oxygen vacancies produced at the surface can diffuse to subsurface sites, resulting in reversible phase transformations in the entire ceria nanoparticle. The ease with which the entire particle can reduce and reoxidize is important in automotive catalysts and intermediate-temperature fuel cells.[35,36] *In situ* EELS in an environmental transmission electron microscope has been employed to determine the local oxidation state of the cerium and thus the degree to which oxygen vacancies are present in cerium-based oxides. This approach has also been employed to investigate surface restructuring and reversible oxygen vacancy ordering under reducing conditions.[37,38]

Figure 6 shows a redox cycle for a CeO_2 crystal during which the temperature was cycled in about 1.5 mbar of H_2.[38] At 693°C, the Ce M_{45} white lines in the energy-loss spectrum reverse, reflecting an abrupt change in the oxidation state of Ce. Simultaneously, superlattice fringes appear in the atomic-resolution image (as shown by the white arrows), and superlattice spots appear in the electron diffraction pattern as a result of the ordering of oxygen vacancies. The reaction is completely reversible, and the structure vanishes upon cooling to 600°C as the ceria reoxidizes. The phase transformation is associated with a doubling of the lattice parameter and the formation of a bcc structure.

The ease with which this redox process takes place can be influenced by doping, and metal nanoparticles can also be employed to enhance the reduction kinetics through a hydrogen-spillover effect.[39] Using ETEM, Sharma et al. found a preferential reduction of ceria in the vicinity of Ni particles at temperatures much lower than the reduction temperature observed for the pure oxide.[39]

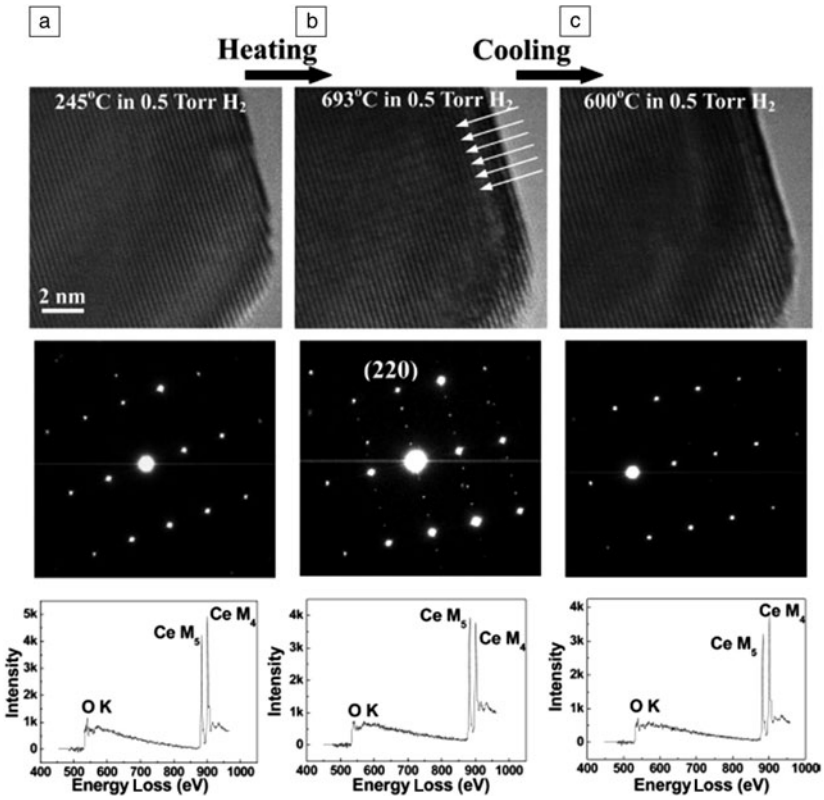


Figure 6. Dynamic changes in atomic-level structure characterized by (top) high-resolution imaging, (middle) electron diffraction, and (bottom) oxidation-state change determined by electron energy-loss spectroscopy at (a) 245°C, (b) 693°C, and (c) 600°C in 1 mbar of H_2 along the $[2\bar{1}1]$ zone axis from the same individual CeO_2 nanoparticle during a redox cycle. After reduction (b), the arrows in the high-resolution image show the new periodicity, and the extra spots along the (220) plane in the electron diffraction pattern also show the superstructure formed during reduction.[38]

Photocatalysts

Photocatalysis, wherein light irradiation provides most of the energy for a reaction, has great potential for solar fuels.[40] To understand structure–reactivity relations at the atomic level, it is necessary to introduce light as a stimulus in the ETEM apparatus. ETEM-compatible light illumination has been developed, and interested readers should see References 41–43 for further information. For example, an ETEM investigation of TiO_2 under water splitting conditions showed that a disorder layer 1–2 monolayers thick formed quickly upon exposure to water and UV (ultraviolet) light.[43] Further analysis showed that this amorphous layer was the hydroxylated surface formed due to the interaction between light-induced oxygen vacancies and adsorbed water molecules.

Catalyst sintering

Deactivation due to sintering is important for many supported metal catalysts that operate at high temperatures, and there is considerable interest in trying to understand the fundamental atomic-level processes involved (see Reference 44 and references therein). There is considerable discussion about the sintering mechanism in the catalysis community because particle sintering can occur through either Ostwald ripening or particle migration and coalescence. However, significant progress has been made with *in situ* observations of catalyst sintering.

Liu et al. investigated the sintering of Pd on an industrial α-Al_2O_3 support in 500 mTorr (0.67 mbar) of H_2O at 700°C over a period of 8 h.[45] The mean particle size increased from 7 nm to 10 nm, and image sequences showed that small particles shrank and larger particles grew, demonstrating that Ostwald ripening was the dominant mechanism in this case. Similar experiments were carried out by Hansen et al. on a steam reforming

https://doi.org/10.1557/mrs.2014.304 Published online by Cambridge University Press

catalyst consisting of Ni particles on a $MgAl_2O_4$ support.[46,47] The sample was reduced *in situ* in flowing H_2 at 500°C, and after reduction, the samples were exposed to either pure H_2 or a mixture of H_2 and H_2O at higher temperatures. Samples exposed to H_2O-containing environments sintered considerably more than those exposed to pure H_2. Challa et al. investigated the sintering of a $Ni/MgAl_2O_4$ methane steam reforming catalyst in a mixture of H_2 and H_2O at 750°C at a few Torr (a few mbar) pressure and found that sintering proceeded mostly by Ostwald ripening.[47,48] They analyzed the evolution of the system to extract energy parameters for a mean-field ripening model and were able to predict ripening behavior over a short time period.

Simonsen and co-workers conducted a series of sintering experiments on Pt particles supported on amorphous Al_2O_3 and SiO_2 films.[49] These systems are considerably simpler than industrial supports and can be used to determine fundamental mechanisms and parameters associated with sintering models. For Pt on Al_2O_3, experiments conducted in 10 mbar of air at a temperature of 650°C showed clear evidence for coarsening taking place through Ostwald ripening over a 7 h period. Simonsen et al. used a mean-field theory to model the rate of change of the distribution with time and found that this gave good agreement with the experimental results, but there were local deviations in certain regions of the support.

Benavidez et al. investigated the sintering of Pt particles on a SiO_2 amorphous film under O_2 at 500°C and of Pd on an amorphous carbon film heated in H_2 at 600°C.[50] In both cases, sintering proceeded by Ostwald ripening, and much of the distribution could be described by mean-field theory. Ostwald ripening was the sintering mechanism for Pt on amorphous planar SiO_2 annealed in air at 650°C, and the data could be well described with a mean-field theory but with local variations in behavior.[51] The authors developed a kinetic model that takes the local mass distribution into account using a Voronoi weighting scheme and were able to make a reasonable prediction of the particle size evolution starting from the initial particle configuration.

Operando transmission electron microscopy

The term *operando* originates from the field of Raman spectroscopy and is used when structure and catalytic activity are detected simultaneously.[52] In a strict sense, the term is applied when structure is determined simultaneously with reaction kinetics. For the current discussion of ETEM, we use the term *operando* or near-*operando* to mean application of ETEM to determine catalyst structure and composition while simultaneously quantitatively detecting the formation of catalytic products. Such an approach should allow structure–reactivity correlations to be determined without the need for *ex situ* reactor studies. Suitable spectroscopic methods must be developed to detect the product gas molecules, and most ETEM instruments are equipped with residual gas analyzers. Giorgio et al. used such a setup to confirm CO conversion to CO_2 over an Au catalyst in experiments performed in a windowed cell reactor in a transmission electron microscope.[30] They were able to correlate the shape of the Au particles with an increase in the CO_2 signal, although they presented no quantitative conversion or activity data. The approach was recently used by Vendelbo et al. to investigate the oscillatory behavior of Pt nanoparticles catalyzing CO oxidation.[53] In this work, the output from a nanoreactor was fed to a residual gas analyzer to identify the onset of oscillatory catalytic behavior. The authors were then able to correlate changes in CO_2 production with changes in particle shape. The results are shown in **Figure 7** and represent a remarkable demonstration of the power of ETEM to determine structure–reactivity correlations in catalysis.

In larger cells associated with differentially pumped ETEM instruments, the detection of catalysis can be more challenging because the volume of the catalyst is small compared to the volume of the reactor. This problem can be addressed by fabricating pellets that can fit in the microscope hot stage and allow increases in catalyst loadings of 10–100 times over conventional TEM preparation such that catalytic products can easily be detected using residual gas analysis (RGA).[54] However, quantification of the mass spectrometry data from RGA in an ETEM apparatus is challenging because the signal might have a nonlinear dependence on gas concentration, and calibrating across different pressures and compositions is difficult. To address this limitation, EELS can be used to quantify the gas composition inside the reaction cell.[55] This approach was employed to detect and quantify reaction products on a Ru-based catalyst performing CO oxidation inside an ETEM instrument.[56] CO_2 has a π^* peak that is 3 eV higher in energy than the

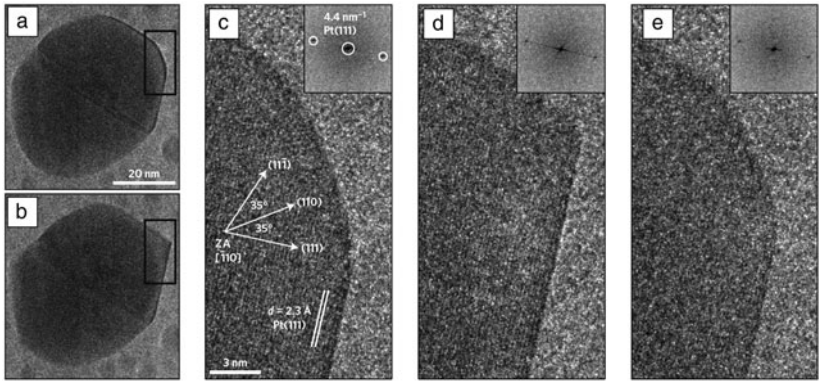


Figure 7. Atomic-scale visualization of dynamic refaceting of a Pt nanoparticle during oscillatory CO oxidation.[53] The Pt particle is viewed along the $[\bar{1}10]$ zone axis (ZA) with a (111) spacing *d* of 2.3 Å, and the area enclosed with the black rectangle is shown at higher magnification in (c–e). The particles show a (a, c, e) rounded or (b, d) more faceted shape as the CO conversion oscillates. Reproduced with permission from Reference 53. © 2014 Nature Publishing Group.

https://doi.org/10.1557/mrs.2014.304 Published online by Cambridge University Press

π* peak from CO, making quantification straightforward. **Figure 8**a shows the change in the energy-loss spectra as a function of temperature when 1 Torr (~1 mbar) of ($2CO + O_2$) was flowed through the microscope reaction cell. At 150°C, a second peak appeared and grew as the catalyst activated and converted the CO to CO_2. The spectra can be quantified to determine the CO conversion in the cell, and the inset shows the CO conversion determined from ETEM EELS.

The quantitative determination of products present in the cell allows relative changes in reaction kinetics to be measured. This is illustrated in Figure 8b for a thermal cycle during CO oxidation over a Ru catalyst.[57] The catalyst is initially in the form of RuO_2 and is heated progressively to 500°C and then cooled to room temperature in flowing CO and O_2. At 300°C, on ramp-up, the CO_2 mole fraction present is 0.04, whereas at the same temperature on ramp-down, the CO_2 mole fraction is 0.3. Because the reactor geometry and catalyst loading remain constant, the change in CO conversion is a consequence of the catalyst activity increasing by a factor of 7.

These results demonstrate that with the *operando* approach, changes in reaction kinetics can be measured. This approach provides a powerful technique for exploring how different *in situ* treatments such as reduction and oxidation can change the activity of a catalyst. *Operando* TEM will allow atomic-level structure to be correlated with changes in relative reaction kinetics and will greatly enhance the determination of structure–reactivity relations.

Conclusions and future outlook

The ability to employ *in situ* and *operando* transmission electron microscopy methods to perform atomic resolution imaging and analysis of nanocatalysts under reaction conditions will continue to evolve and improve in the years ahead. Microelectromechanical systems-based windowed cells have already allowed the imaging of nanocatalysts with atomic resolution at pressures above one atmosphere (1 bar). It may only be a matter of time before differentially pumped systems can operate at higher pressures. Other types of stimuli are also being investigated, which will open up new opportunities for catalytic investigations. Electrical biasing of samples is now possible, providing potential opportunities for investigating electrocatalytic processes. Implementing light sources has made *in situ* investigation of photocatalytic and electrophotocatalytic systems feasible. Probing atomic level processes in catalysts under reaction conditions is exciting and is sure to be highly productive.

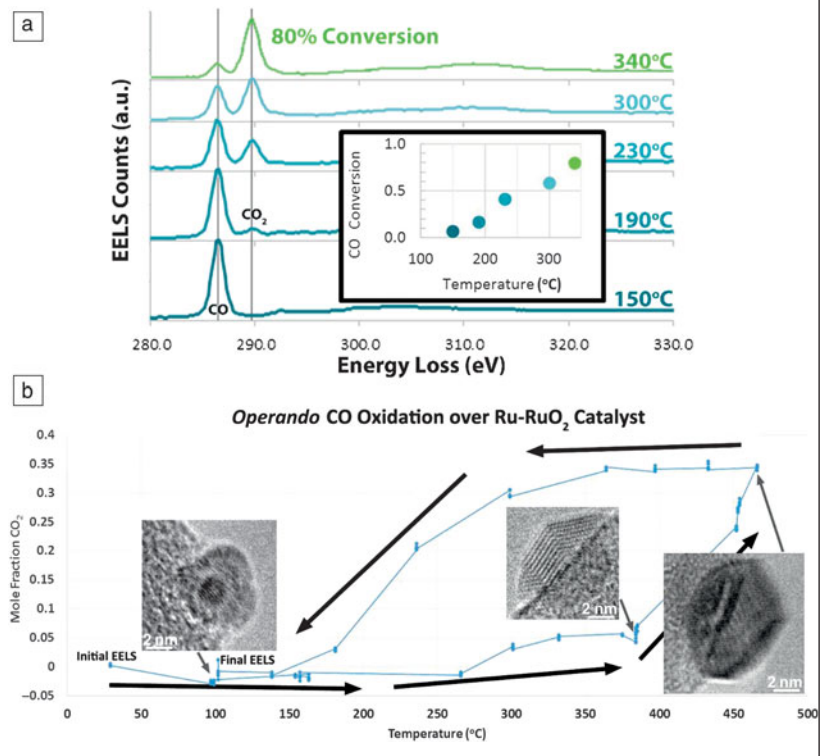


Figure 8. (a) Electron energy-loss spectroscopy (EELS) carbon K-edge from the gas phase recorded as a function of temperature from a CO oxidation *operando* experiment with a glass fiber pellet.[54] (b) Results from a CO oxidation experiment in which a Ru–RuO_2 catalyst was heated from room temperature to 460°C and then cooled to 100°C in CO and O_2. Inset: High-resolution images recorded at different points in the heating and cooling cycle. The initial RuO_2 converts to hcp Ru metal at around 500°C, giving a much more active form of the catalyst.[57] Reproduced with permission from References 54 and 57. © 2013 Cambridge University Press.

Acknowledgments

P.A.C. acknowledges financial support from the US NSF (CTS-0306688, CBET 0553445, and CBET 1134464) and US Department of Energy (DE-SC0004954). He also gratefully acknowledges the use of facilities within the LeRoy Eyring Center for Solid State Science at Arizona State University. T.W.H. acknowledges the A.P. Møller and Chastine McKinney Møller Foundation for its contribution toward the establishment of the Center for Electron Nanoscopy in the Technical University of Denmark. Both authors are grateful to all of the students, postdocs, and colleagues with whom they have collaborated over the years.

References

1. G. Ertl, H. Knözinger, J. Weitkamp, *Handbook of Heterogeneous Catalysis* (VCH, Weinheim, Germany, 1997).
2. G.A. Somorjai, Y. Li, *Introduction to Surface Chemistry and Catalysis* **2**nd ed.(Wiley-VCH, Weinheim, Germany, 2010), p. 442.
3. T.W. Hansen, J.B. Wagner, P.L. Hansen, S. Dahl, H. Topsoe, C.J.H. Jacobson, *Science* **294**, 1508 (2001).
4. R.T.K. Baker, M.A. Barber, P.S. Harris, F.S. Feates, R.J. White, *J. Catal.* **26**, 51 (1972).
5. R.T.K. Baker, P.S. Harris, R.B. Thomas, R.J. Waite, *J. Catal.* **30**, 86 (1973).
6. R. Sharma, *J. Mater. Res.* **20** (7), 1695 (2005).
7. P.L. Gai, E.D. Boyes, in *In-Situ Microscopy in Materials Research*, P.L. Gai, Ed. (Kluwer Academic Publishers, Dordrecht, The Netherlands, 1997), pp. 123–146.
8. P.L. Gai, E.D. Boyes, S. Helveg, P.L. Hansen, S. Giorgio, C.R. Henry, *MRS Bull.* **32** (12), 1044 (2007).
9. R. Sharma, P.A. Crozier, in *Handbook of Microscopy for Nanotechnology*, N. Yao, Z.L. Wang, Eds. (Kluwer Academic Publishers, New York, 2005), pp. 531–563.
10. S. Giorgio, S. Sao Joao, S. Nitsche, D. Chaudanson, G. Sitja, C.R. Henry, *Ultramicroscopy* **106**, 503 (2006).

https://doi.org/10.1557/mrs.2014.304 Published online by Cambridge University Press

11. G.M. Parkinson, *Catal. Lett.* **2**, 303 (1989).
12. J.F. Creemer, S. Helveg, G.H. Hoveling, S. Ullmann, A.M. Molenbroek, P.M. Sarro, H.W. Zandbergen, *Ultramicroscopy* **108**, 993 (2008).
13. T. Alan, T. Yokosawa, J. Gaspar, G. Pandraud, O. Paul, F. Creemer, P.M. Sarro, H.W. Zandbergen, *Appl. Phys. Lett.* **100**, 4 (2012).
14. T. Yokosawa, T. Alan, G. Pandraud, B. Dam, H. Zandbergen, *Ultramicroscopy* **112**, 47 (2012).
15. S.B. Vendelbo, P.J. Kooyman, J.F. Creemer, B. Morana, L. Mele, P. Dona, B.J. Nelissen, S. Helveg, *Ultramicroscopy* **133**, 72 (2013).
16. T.W. Hansen, J.B. Wagner, R.E. Dunin-Borkowski, *Mater. Sci. Technol.* **26**, 1338 (2010).
17. P.R. Swann, N.J. Tighe, paper presented at the 5th European Congress on Electron Microscopy., Manchester, UK, Institute of Physics, Royal Microscopical Society, 1972.
18. R.C. Doole, G.M. Parkinson, J.M. Stead, *Inst. Phys. Conf. Ser.* **119**, 157 (1991).
19. T.C. Lee, D.K. Dewald, J.A. Eades, I.M. Robertson, H.K. Birnbaum, *Rev. Sci. Instrum.* **62**, 1438 (1991).
20. E.D. Boyes, P.L. Gai, *Ultramicroscopy* **67**, 219 (1997).
21. R. Sharma, K. Weiss, *Microsc. Res. Tech.* **42**, 270 (1998).
22. P.L. Hansen, J.B. Wagner, *Proc. 12th Eur. Congr. Electron Microsc.* (Czechoslovak Society for Electron Microscopy, Brno, Czech Republic, 2000), vol. 2, pp. 537–538.
23. J.R. Jinschek, S. Helveg, *Micron* **43**, 1156 (2012).
24. P. Li, J. Liu, N. Nag, P.A. Crozier, *J. Catal.* **262**, 73 (2009).
25. R. Banerjee, P.A. Crozier, *J. Phys. Chem. C* **116**, 11486 (2012).
26. R. Dehghan, T.W. Hansen, J.B. Wagner, A. Holmen, E. Rytter, O. Borg, J.C. Walmsley, *Catal. Lett.* **141**, 754 (2011).
27. H.L.L. Xin, E.A. Pach, R.E. Diaz, E.A. Stach, M. Salmeron, H.M. Zheng, *ACS Nano* **6**, 4241 (2012).
28. Q. Jeangros, A. Faes, J.B. Wagner, T.W. Hansen, U. Aschauer, J. Van Herle, A. Hessler-Wyser, R.E. Dunin-Borkowski, *Acta Mater.* **58**, 4578 (2010).
29. M. Haruta, N. Yamada, T. Kobayashi, S. Iijima, *J. Catal.* **115**, 301 (1989).
30. S. Giorgio, M. Cabie, C.R. Henry, *Gold Bull.* **41**, 167 (2008).
31. T. Uchiyama, H. Yoshida, Y. Kuwauchi, S. Ichikawa, S. Shimada, M. Haruta, S. Takeda, *Angew. Chem. Int. Ed.* **50**, 10157 (2011).
32. H. Yoshida, Y. Kuwauchi, J.R. Jinschek, K.J. Sun, S. Tanaka, M. Kohyama, S. Shimada, M. Haruta, S. Takeda, *Science* **335**, 317 (2012).
33. S. Chenna, R. Banerjee, P.A. Crozier, *ChemCatChem* **3**, 1051 (2011).
34. S. Chenna, P.A. Crozier, *Micron* **43**, 1188 (2012).
35. R.J. Gorte, J.M. Vohs, in *Annual Review of Chemical and Biomolecular Engineering*, J.M. Prausnitz, Ed. (Annual Reviews, Palo Alto, CA, 2011), vol. 2, pp. 9–30.
36. M.P. Yeste, J.C. Hernandez, S. Bernal, G. Blanco, J.J. Calvino, J.A. Perez-Omil, J.M. Pintado, *Catal. Today* **141**, 409 (2009).
37. P.A. Crozier, R. Wang, R. Sharma, *Ultramicroscopy* **108**, 1432 (2008).
38. R. Wang, P.A. Crozier, R. Sharma, *J. Phys. Chem. C* **113**, 5700 (2009).
39. V. Sharma, P.A. Crozier, R. Sharma, J.B. Adams, *Catal. Today* **180**, 2 (2012).
40. A. Kudo, Y. Miseki, *Chem. Soc. Rev.* **38**, 253 (2009).
41. F. Cavalca, A.B. Laursen, B.E. Kardynal, R.E. Dunin-Borkowski, S. Dahl, J.B. Wagner, T.W. Hansen, *Nanotechnology* **23**, 075705 (2012).
42. B.K. Miller, P.A. Crozier, *Microsc. Microanal.* **19**, 461 (2013).
43. L.X. Zhang, B.K. Miller, P.A. Crozier, *Nano Lett.* **13**, 679 (2013).
44. A.K. Datye, *Catal. Today* **111**, 59 (2006).
45. R.-J. Liu, P.A. Crozier, C.M. Smith, D.A. Hucul, J. Blackson, G. Salaita, *Appl. Catal. A* **282**, 111 (2005).
46. T.W. Hansen, A.T. Delariva, S.R. Challa, A.K. Datye, *Acc. Chem. Res.* **46**, 1720 (2013).
47. A.T. DeLaRiva, T.W. Hansen, S.R. Challa, A.K. Datye, *J. Catal.* **308**, 291 (2013).
48. S.R. Challa, A.T. Delariva, T.W. Hansen, S. Helveg, J. Sehested, P.L. Hansen, F. Garzon, A.K. Datye, *J. Am. Chem. Soc.* **133**, 20672 (2011).
49. S.B. Simonsen, I. Chorkendorff, S. Dahl, M. Skoglundh, J. Sehested, S. Helveg, *J. Am. Chem. Soc.* **132**, 7968 (2010).
50. A.D. Benavidez, L. Kovarik, A. Genc, N. Agrawal, E.M. Larsson, T.W. Hansen, A.M. Karim, A.K. Datye, *ACS Catal.* **2**, 2349 (2012).
51. S.B. Simonsen, I. Chorkendorff, S. Dahl, M. Skoglundh, J. Sehested, S. Helveg, *J. Catal.* **281**, 147 (2011).
52. M.A. Bañares, I.E. Wachs, *J. Raman Spectrosc.* **33**, 359 (2002).
53. S.B. Vendelbo, C.F. Elkjær, H. Falsig, I. Puspitasari, P. Dona, L. Mele, B. Morana, B.J. Nelissen, R. van Rijn, J.F. Creemer, P.J. Kooyman, S. Helveg, *Nat. Mater.* **13**, 884 (2014).
54. B.K. Miller, P.A. Crozier, *Microsc. Microanal.* **20**, 815 (2014).
55. P.A. Crozier, S. Chenna, *Ultramicroscopy* **111**, 177 (2011).
56. S. Chenna, P.A. Crozier, *ACS Catal.* **2**, 2395 (2012).
57. B.K. Miller, P.A. Crozier, *Microsc. Microanal.* **20**, 1564 (2014). □

SAVE THESE DATES APRIL 25-30, 2015
SANTA CLARA 58th Annual Technical Conference Santa Clara Convention Center, CA, USA
SVC TECHCON 2015
SOCIETY OF VACUUM COATERS
APRIL 27-30 TECHNICAL PROGRAM featuring a Symposium on
Coating Technologies for the Interconnected Age
ADVANCING MOBILITY, DURABILITY AND PERFORMANCE OF MOBILE ELECTRONICS
The SVC Technical Advisory Committees will explore the Symposium topic in depth together with our traditional Technical Sessions.
APRIL 25-30 EDUCATION PROGRAM Problem-Solving Tutorial Courses
APRIL 28-29 EQUIPMENT EXHIBIT Dedicated to Vacuum Coating Technologies
APRIL 26-30 INTERACTIVE NETWORKING Forums and Discussion Groups
SPOTLIGHT SESSIONS
Technical Poster Presentations: with 3-Minute Oral Presentations
Heuréka! Post-Deadline Recent Developments: Featuring Late-Breaking Technology
Business Topics: Beyond Vacuum Coating... New Ideas Making Your Business Better
Vendor Innovators Showcase: 10-Minute Vendor Presentations during the Exhibit
Abstracts Accepted for Spotlight Sessions **until March 1, 2015**
REGISTER ON-LINE AT **www.svc.org**
FOR MORE INFORMATION
SVCINFO@SVC.ORG . 505-856-7188 . WWW.SVC.ORG

https://doi.org/10.1557/mrs.2014.304 Published online by Cambridge University Press